Available online at www.sciencedirect.com
SCIENCE DIRECT
Polymer 46 (2005) 4060–4067
polymer
www.elsevier.com/locate/polymer

Crystallization behavior of poly(ε-caprolactone) blocks starting from polyethylene lamellar morphology in poly(ε-caprolactone)-*block*-polyethylene copolymers

Shuichi Nojima[a,*], Yosuke Akutsu[a], Michiaki Akaba[a], Satoshi Tanimoto[b]

[a]*Department of Polymer Chemistry, Tokyo Institute of Technology, H-125, 2-12-1 Ookayama, Meguro-Ku, Tokyo 152-8552, Japan*
[b]*Department of Materials Science, The University of Shiga Prefecture, 230 Hassaka-cho, Hikone, Shiga 522-8533, Japan*

Received 9 September 2004; received in revised form 20 January 2005; accepted 2 February 2005
Available online 20 April 2005

Abstract

The crystallization behavior of poly(ε-caprolactone) (PCL) blocks starting from a solid lamellar morphology formed in advance by the crystallization of polyethylene (PE) blocks (PE lamellar morphology) in a PCL-*b*-PE diblock copolymer was investigated by differential scanning calorimetry (DSC), small-angle X-ray scattering with synchrotron radiation (SR-SAXS), and polarized optical microscope (POM). The crystallization behavior was quantitatively compared with that of a PCL-*block*-polybutadiene copolymer, where the crystallization of PCL blocks started from a rubbery lamellar microdomain. DSC and SR-SAXS results revealed that the crystallization rate of PCL blocks in PCL-*b*-PE increased drastically with decreasing crystallization temperature T_c and the Avrami exponent depended significantly on T_c. SR-SAXS curves during the crystallization of PCL blocks at high T_c showed a bimodal scattering character, that is, the peak position moved discontinuously with crystallization time. At low T_c, on the other hand, no shift of the SAXS peak position was observed. The macroscopic change in morphology was detected only at high T_c by POM observations. These experimental results for the crystallization behavior of PCL blocks in PCL-*b*-PE all support our previous conclusions obtained by static measurements; the crystallization mechanism at low T_c is completely different from that at high T_c, that is, the PCL blocks crystallize within the PE lamellar morphology at low T_c while the crystallization of PCL blocks at high T_c yields a morphological transition from the PE lamellar morphology into a new solid morphology.

Keywords: Crystalline–crystalline diblock copolymer; Lamellar morphology; Crystallization behavior

1. Introduction

The crystallization behavior of low-molecular-weight crystalline–amorphous diblock copolymers is interesting from the viewpoint of morphology formation because a microdomain structure turns into a completely different lamellar morphology, an alternating structure consisting of thin crystals and amorphous layers. This behavior has usually been observed by time-resolved small-angle X-ray scattering with synchrotron radiation (SR-SAXS) [1–7], and the results are analyzed by the Avrami equation widely used for homopolymer crystallization. These results show that the crystallization behavior of block copolymers is qualitatively similar to that of homopolymers, that is, pre-existing microdomains do not substantially affect the subsequent crystallization of constituent blocks.

The crystallization behavior of crystalline–crystalline diblock copolymers would be more complicated because two kinds of crystallization work cooperatively when the copolymer is quenched from the microphase-separated melt into various temperatures below the melting temperatures of both blocks. When the melting temperatures of both blocks are close enough such as poly(ethylene oxide)-*block*-poly(ε-caprolactone) copolymers, we expect a simultaneous crystallization of both the blocks by quenching, and the thermal analysis and microscopic observation have revealed a unique crystallization behavior [8–13]. When the melting temperature of one block is far from the other, on the other hand, we have a completely different crystallization; one block crystallizes in advance to result in some morphology and subsequently the other block crystallizes starting from

* Corresponding author. Tel.: +81 3 5734 2132; fax: +81 3 5734 2888.
E-mail address: snojima@polymer.titech.ac.jp (S. Nojima).

0032-3861/$ - see front matter © 2005 Elsevier Ltd. All rights reserved.
doi:10.1016/j.polymer.2005.02.075

this morphology. Though the crystallization behavior and resulting morphology of such cases have been studied for some diblock and triblock copolymers [14–20], they are not quantitatively understood so far.

In our previous study [20], we synthesized various poly(ε-caprolactone)-*block*-polyethylene (PCL-*b*-PE) diblock copolymers and investigated the morphology formed by the crystallization of both blocks, where the melting temperature of PCL blocks $T_{m,PCL}$ was ca. 56 °C and that of PE blocks $T_{m,PE}$ was 95 °C. The PE block crystallized first during quenching from the microphase-separated melt into various crystallization temperatures T_c below $T_{m,PCL}$, and, therefore, the solid lamellar morphology consisting of PE crystals and amorphous layers (PE lamellar morphology) always existed prior to the crystallization of PCL blocks. We found that the resulting morphology depended significantly on T_c. That is, at low T_c, PCL blocks crystallized within the PE lamellar morphology and eventually it was preserved throughout the crystallization process of PCL blocks. At high T_c, on the other hand, the crystallization of PCL blocks destroyed the PE lamellar morphology to result in a new lamellar morphology favorable for the crystallization of PCL blocks. Therefore, we can expect that the crystallization behavior of PCL blocks at high T_c will be completely different from that at low T_c.

In this study, we clarify the crystallization behavior of PCL blocks starting from the PE lamellar morphology by differential scanning calorimetry (DSC), SR-SAXS, and polarized optical microscope (POM). In particular, the difference in crystallization behavior between low and high T_c will be emphasized. The results are compared with the crystallization behavior of a PCL-*block*-polybutadiene (PCL-*b*-PB) copolymer with the same molecular characteristics, where the crystallization of PCL blocks starts from the rubbery lamellar microdomain to yield a morphological transition into the solid (or crystallized) lamellar morphology at all T_c.

2. Experimental

2.1. Samples

Samples used in this study are double crystalline poly(ε-caprolactone)-*block*-polyethylene (PCL-*b*-PE) diblock copolymers, which were obtained by the hydrogenation of PCL-*block*-polybutadiene (PCL-*b*-PB) diblocks. The methods of PCL-*b*-PB synthesis and hydrogenation were described in our previous paper [1,20]. We also used PCL-*b*-PB just before the hydrogenation to compare the crystallization behavior of PCL blocks with that of PCL-*b*-PE. A major difference between PCL-*b*-PE and PCL-*b*-PB is the pre-existing morphology from which PCL blocks start to crystallize; the solid PE lamellar morphology exists in PCL-*b*-PE while the rubbery lamellar microdomain in PCL-*b*-PB.

The molecular characteristics of PCL-*b*-PE and PCL-*b*-PB are shown in Table 1, where $T_{m,PE}$ is ca. 95 °C and $T_{m,PCL}$ is ca. 56 °C. A3 and B3 were mainly used to investigate the crystallization behavior of PCL blocks by DSC, SR-SAXS, and POM, but A2 was supplementally used only for SR-SAXS measurements because the morphological transition of A2 at high T_c was more distinct compared with that of A3 (Fig. 5) owing to the SAXS peak appearing at higher-angle. The total number-averaged molecular weight M_n is less than 18,000 for all copolymers, so that the microdomain structure does not preserve by the crystallization of PE and/or PCL blocks when the sample is quenched from the microphase-separated melt [21].

2.2. DSC measurements

The sample was quenched from the melt (ca. 130 °C) into various crystallization temperatures T_c ranging from 30 to 45 °C ($<T_{m,PCL}$) at a maximum cooling rate (=500 °C/min) and annealed at T_c for a prescribed time t_c, where PE blocks already crystallized during quenching to yield the PE lamellar morphology. A Perkin–Elmer DSC Pyris I was used with a heating rate of 10 °C/min to obtain the crystallinity of PCL blocks χ_{PCL} as a function of t_c, where the difference between $T_{m,PCL}$ and $T_{m,PE}$ is large enough, so that χ_{PCL} could be accurately evaluated (Fig. 1(a)). χ_{PCL} was calculated from the endothermic area by assuming that the heat of fusion for perfect PCL crystals was 135.44 J/g [22]. Note that χ_{PCL} might include a minor contribution from the re-crystallization of PCL blocks during heating process.

2.3. SR-SAXS measurements

The SR-SAXS experiment was carried out at Photon Factory in High-Energy Accelerator Research Organization, Tsukuba, Japan, with a small-angle X-ray equipment for solution (SAXES) installed at beam line BL-10C. Details of the optics and the instrumentation were described elsewhere [23,24]. The incident beam intensity with wave length $\lambda=0.1488$ nm was monitored at before and after the sample by two ionization chambers for the evaluation of frame-by-frame transmission factors of the sample and also for the correction of a minor decrease in intensity during measurements. The detector was a one-dimensional position sensitive proportional counter (PSPC) and data accumulation time was 10 s to get each SAXS curve during dynamic measurements. The background scattering and the Lorentz factor were taken into account when the spacing of alternating structures was evaluated.

2.4. POM observations

The macroscopic change in morphology by the crystallization of PCL blocks was observed at various T_c as a function of t_c by a polarized optical microscope (Olympus

Table 1
Molecular characteristics of PCL-*b*-PE and PCL-*b*-PB copolymers

Notation	Sample	Total, M_n[a]	M_w/M_n[b]	PCL:PE (vol%)[c]	EB (mol%)[c]	$T_{m,PCL}$ (°C)[d]	$T_{m,PE}$ (°C)[d]
A3	PCL-*b*-PE	18,000	1.18	51:49	5	56	95
B3	PCL-*b*-PB	17,000	1.18	52:48	5	55	–
A2	PCL-*b*-PE	11,000	1.09	69:31	6	55	97

[a] Determined by membrane osmometry.
[b] Determined by GPC.
[c] Determined by ^{1}H NMR.
[d] Determined by DSC for the samples crystallized at room temperature.

BX-50) with a temperature-controlled hot stage (Linkam LTS-350). The film thickness prepared by a solution-casting method was ca. 0.02 mm for all samples. The morphological change during the crystallization of PCL blocks was monitored between crossed polarizers for qualitative comparison at different T_c.

3. Results and discussion

3.1. DSC results

Fig. 1 shows DSC melting curves for A3 (a) and B3 (b) isothermally crystallized at 42 °C during various crystallization times t_c indicated on each curve. The endothermic peak at ca. 56 °C arising from the melting of PCL blocks grows with increasing t_c for both cases. However, the diffuse endothermic peak at ca. 96 °C arising from the melting of PE blocks (Fig. 1(a)) does not depend on t_c, that is the crystallinity of PE blocks χ_{PE} is constant (ca. 24 wt% against whole PE blocks in A3) irrespective of t_c, indicating that the crystallization of PE blocks has completely finished when the sample arrives at 42 °C from the microphase-separated melt.

We obtained the t_c dependence of χ_{PCL} from the peak area, and then evaluated the half-crystallization time $\tau_{1/2}$, i.e. time necessary to reach the half of final crystallinity of PCL blocks, as a function of T_c for A3 and B3. The inverse of $\tau_{1/2}$, which is a measure of the crystallization rate of PCL blocks, is plotted against T_c in Fig. 2, where the crystallization rate of PCL blocks in A3 is almost equal to that in B3 at high T_c (>45 °C) but the difference increases significantly with decreasing T_c. That is, the crystallization rate in PCL-*b*-PE increases drastically with decreasing T_c compared with the case of PCL-*b*-PB. It is known from our previous studies [2,21] that low-molecular-weight PCL-*b*-PB copolymers take a morphological transition from a rubbery microdomain into a solid lamellar morphology by the crystallization of PCL blocks at all T_c, and the crystallization rate increases steadily with decreasing T_c. Therefore, the drastic increase of crystallization rate in PCL-*b*-PE suggests the change in crystallization mechanism of PCL blocks at low T_c. Thus, the large difference in crystallization rate between PCL-*b*-PE and PCL-*b*-PB at low T_c qualitatively supports our conclusion previously obtained by static measurements for the final morphology of A3 [20], that is, PCL blocks crystallize within the PE lamellar morphology at low T_c (<30 °C) while the morphological transition occurs at high T_c (>30 °C).

Hamley et al. recently investigated the crystallization behavior of a high-molecular-weight crystalline–crystalline diblock copolymer, poly(*p*-dioxanone)-*block*-PCL (PPDX-*b*-PCL) [17]. They found that the crystallization rate of PCL blocks was accelerated by the presence of crystallized PPDX blocks, and concluded that the crystallized PPDX acted to nucleate PCL blocks, so that the heterogeneous

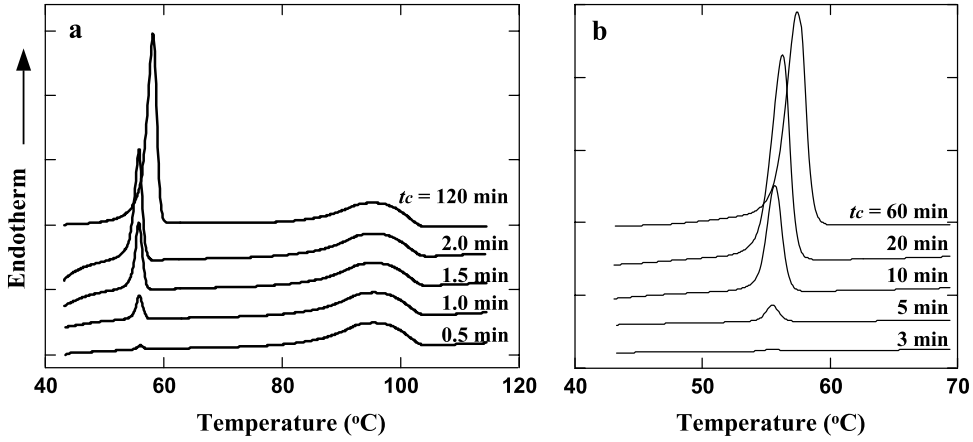

Fig. 1. DSC melting curves for A3 (a) and B3 (b) isothermally crystallized at 42 °C as a function of crystallization time t_c indicated on each curve. The DSC curves are shifted upward successively for legibility.

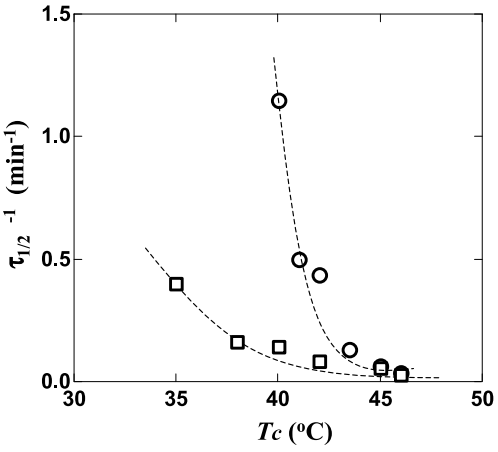

Fig. 2. Inverse of half-crystallization time $\tau_{1/2}$, obtained from DSC measurements for A3 (circle) and B3 (square), plotted against crystallization temperature T_c.

crystallization of PCL blocks was always observed within a confined space. The acceleration of crystallization rate with decreasing T_c is also recently reported for high-molecular-weight crystalline–amorphous diblocks [25,26]. Sakurai et al. for example, investigated the crystallization behavior of a flow-oriented polyethylene-*block*-(atactic-polypropylene) (PE-*b*-PP), and found that the crystallization rate of PE blocks increased significantly with decreasing T_c and also that spherulites could grow only at high T_c, that is, the crystallized lamellar microdomain did not coexist with the spherulitic morphology at all T_c. They concluded that a large number of nuclei prevented the transformation of confined microdomains into spherulites at low T_c. The T_c dependence of crystallization rate observed in their diblock is phenomenologically similar to that in our diblock. The substantial difference in factors controlling the crystallization behavior between crystalline–amorphous and crystalline–crystalline diblocks will be discussed later.

3.2. SR-SAXS curves

Fig. 3 shows time-resolved SAXS curves for A3 quenched from 130 °C into 42 °C. A sharp diffraction arising from the lamellar microdomain (at $t_c = 0$ s) turns quickly into a small scattered peak with a considerable shift of peak position to the low angle, indicating the PE lamellar morphology has formed by the crystallization of PE blocks. After some induction time, the peak intensity increases gradually with increasing t_c, which arises from the crystallization of PCL blocks starting from the PE lamellar morphology. Fig. 4 highlights the change of the SAXS peak with t_c, that is intensity (a), spacing (b), and full width at half maximum (FWHM) (c) of the peak are plotted against t_c for A3 crystallized at 42 °C. The significant change in intensity, spacing, and FWHM between $t_c = 1000$ and 2000 s is intuitively explained if we assume that the PE lamellar morphology deforms moderately by the crystallization of

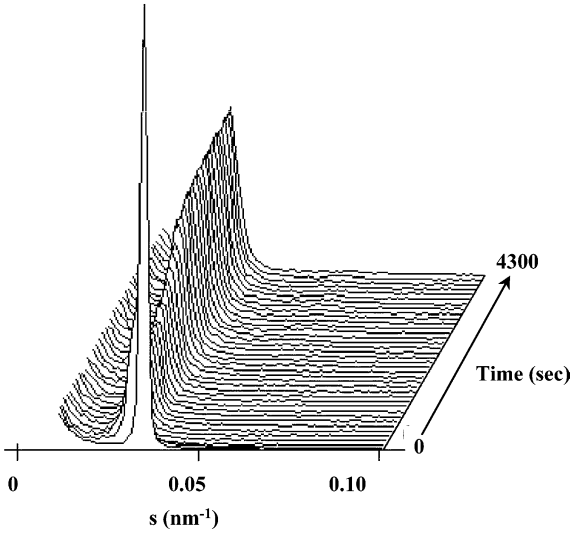

Fig. 3. Time-resolved SAXS curves during the crystallization of PCL blocks when A3 is quenched from the microphase-separated melt into $T_c =$ 42 °C.

PCL blocks. Here, we measure the crystallization behavior of A2 as well as A3 to confirm the generality of Fig. 4, because the SAXS peak appears at higher-angles for A2 and, therefore, we can clearly understand the change in SAXS curves with increasing t_c.

The inset of Fig. 5 shows the change in FWHM for A2 crystallized at 42 °C, where it increases first, takes a maximum (indicated by an arrow in the inset), and finally decreases with t_c. Fig. 5 shows typical SAXS curves at t_c

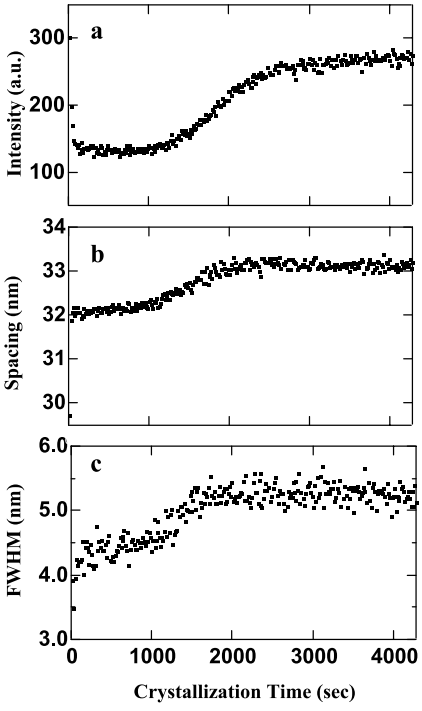

Fig. 4. Intensity (a), spacing (b), and FWHM (c) for the SAXS peak plotted against crystallization time t_c for A3 crystallized at 42 °C.

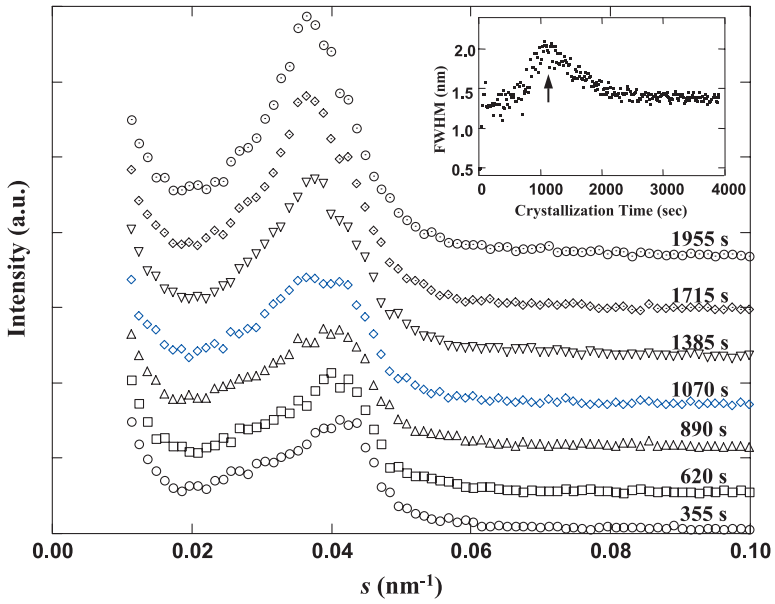

Fig. 5. SAXS curves at each t_c around the maximum of FWHM for A2 quenched from the melt into 42 °C. The SAXS curve at $t_c = 1070$ °C s shows a bimodal character. The inset shows the t_c dependence of FWHM for A2.

around the maximum of FWHM, where we can distinctly see a bimodal SAXS curve at $t_c = 1070$ s. This fact means that the original SAXS peak does not move continuously to the lower-angle but there exist two peaks with their angular positions being very close. The higher-angle peak is gradually replaced with the lower-angle peak as PCL blocks crystallize, which suggests that the PE lamellar morphology is replaced by a new morphology. The molecular weight of A3 is higher than that of A2 and, therefore, SAXS peaks for A3 appear at the lower-angle, which shrinks the difference in angular position between two peaks and eventually we cannot observe two peaks at all.

The experimental results described above were observed only at high T_c for A2 and A3. At low T_c, on the other hand, the peak intensity increased, but FWHM was constant and the peak position did not move with t_c at all. Therefore, the final spacing after the crystallization of PCL blocks was exactly equal to that of the PE lamellar morphology. This fact indicates that the pre-existing PE lamellar morphology preserves throughout crystallization and eventually PCL blocks crystallize within this morphology. These experimental facts both at high and low T_c are consistent with our previous conclusion obtained from static measurements [20].

3.3. Analysis of SR-SAXS curves

The half-crystallization time $\tau^*_{1/2}$ can be evaluated from the t_c dependence of the SAXS peak intensity. Because the peak arising from the crystallization of PCL blocks was overlapped with the higher-angle peak (arising from the PE lamellar morphology) at high T_c (Fig. 5), we decomposed this combined peak into two by assuming the Lorentz function for each peak,

$$I(s) = \frac{2A}{\pi W}\left[1 + \frac{4}{W^2}(s - s_{\max})^2\right]^{-1} \quad (1)$$

where W is FWHM of the peak, A is proportional to the peak area, and $s_{\max}$ is the maximum value of s. This function is usually used to approximate diffraction intensities from crystalline materials in order to characterize each peak [27], and is empirically used with no theoretical basis. The angular position of two peaks was extremely close for A3 at high T_c, so that the result of peak decomposition contained much error. However, because we had the initial and final values of the peak intensity, $\tau^*_{1/2}$ evaluated by this procedure was adequately reliable. The peak intensity thus obtained showed a sigmoidal variation against t_c, which is usually observed in homopolymer crystallization [28,29].

Fig. 6 shows the plot of $1/\tau^*_{1/2}$ against T_c, where $1/\tau^*_{1/2}$ of A3 is identical with that of B3 at high T_c but the difference increases significantly with decreasing T_c. One remarkable difference between Figs. 2 and 6 is the temperature at which the deviation between A3 and B3 is notable (45 °C for Fig. 2 and 38 °C for Fig. 6). The other important difference is the T_c dependence of $\tau^{-1}_{1/2}$ (or $\tau*^{-1}_{1/2}$) at low T_c; it increases exponentially with decreasing T_c in Fig. 2 while it increases linearly in Fig. 6. These difference may arise from the difference in measuring method between $\tau_{1/2}$ and $\tau^*_{1/2}$. That is, the DSC result might include an additional crystallization of PCL blocks during heating process while the SR-SAXS measurement pursues the neat crystallization process of PCL blocks. Therefore, a quantitative comparison between Figs. 2 and 6 needs information about the morphological change during heating, which will soon appear in a forthcoming paper. In summary,

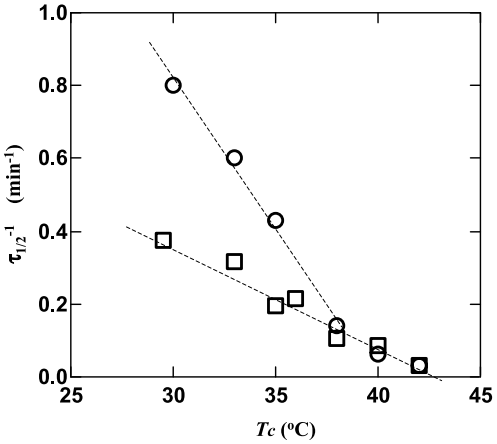

Fig. 6. Inverse of half-crystallization time $\tau^*_{1/2}$, obtained from SR-SAXS measurements for A3 (circle) and B3 (square), plotted against crystallization temperature T_c.

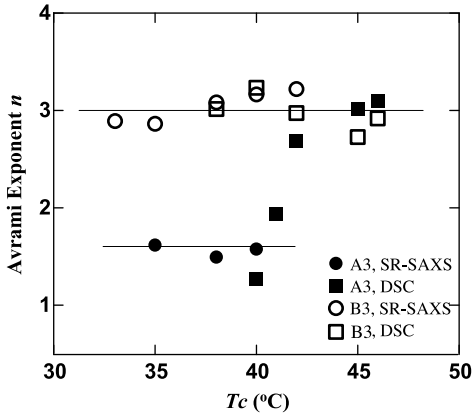

Fig. 7. The Avrami exponent n, evaluated from DSC measurements (square) and SR-SAXS measurements (circle) for A3 (closed symbols) and B3 (open symbols), plotted against T_c.

Fig. 6 also demonstrates that the crystallization mechanism of A3 changes with T_c because B3 takes a morphological transition from the rubbery lamellar microdomain into the solid lamellar morphology at all T_c.

The crystallization behavior of materials is usually analyzed by the Avrami equation [30], which is widely used for homopolymer crystallization [28,29],

$$X(t_c) = 1 - \exp[-(Kt_c)^n] \quad (2)$$

where K is a crystallization-rate constant and n is the Avrami exponent expressing the mode of crystallization. $X(t_c)$ is the normalized crystallinity (in volume fraction) at t_c (i.e. crystallinity at t_c divided by that at $t_c = \infty$), and can be evaluated from DSC results (Fig. 1) or SR-SAXS results (Fig. 4(a)) independently. In the treatment of SR-SAXS results, we could not quantitatively analyze bimodal SAXS curves for A3 at high T_c owing to the reason described in the evaluation of $\tau^*_{1/2}$, so that we analyzed SR-SAXS results obtained only at low T_c, where the peak position did not change with T_c. In addition, the development of endothermic peak area in DSC measurements was too fast to be detected at low T_c, and, therefore, we could not analyze DSC results obtained at low T_c both for A3 and B3.

Fig. 7 shows the T_c dependence of n evaluated from SR-SAXS and DSC results for A3 and B3, where n for B3 at all T_c and A3 at high T_c (>42 °C) is about three, indicating a heterogeneous nucleation in 3D space. This is consistent with the values obtained for many crystalline homopolymers and also block copolymers in which morphological transition occurs by the crystallization of constituent blocks [2,5]. On the other hand, n for A3 at low T_c (<40 °C) is considerably small and the average value is ca. 1.6. When the crystallization is completely confined within a spherical microdomain, it is reported that n is reduced to one or less [31,32]; an unusually small n seems to be characteristic for the crystallization in confined space. Fig. 7 suggests that the crystallization of PCL blocks in A3 brings about the morphological transition at high T_c (>42 °C) while it occurs within the pre-existing PE lamellar morphology in low T_c (<40 °C), which is consistent with our previous observations for the final morphology in various PCL-*b*-PE copolymers [20].

3.4. POM observations

Macroscopic change in morphology by the crystallization of PCL blocks was also observed by POM, and results are shown in Fig. 8 for A3 crystallized at 49 °C ((b) and (c)) and 7 °C ((d) and (e)) for a qualitative comparison. Fig. 8(a) shows the morphology at 70 °C, where only PE blocks crystallize but we cannot observe any significant pattern in POM pictures since the crystallinity of PE blocks is fairly small (12 wt% against whole system). When PCL blocks are crystallized at 49 °C, we can observe the development of white aggregates and their area fraction increases with increasing t_c. This aggregate is far from the distinct spherulite sometimes observed in neat crystalline–amorphous diblocks [33], and, therefore, difficult to be quantitatively analyzed. However, the white aggregate appears only by the crystallization of PCL blocks at high T_c, suggesting the morphological transition occurs only at high T_c. When PCL blocks are crystallized at 7 °C (Fig. 8(d)), on the other hand, no change in POM pictures is observed at $t_c = 30$ min, indicating that further macroscopic re-organization in morphology does not take place by the crystallization of PCL blocks, which confirms that PCL blocks crystallize within the PE lamellar morphology. In summary, the macroscopic observation also indicates the difference in crystallization mechanism of PCL blocks at high T_c ($=49$ °C) and low T_c ($=7$ °C).

To investigate the possibility of further crystallization of PCL blocks crystallized at 7 °C for 30 min, A3 was subsequently brought into 45 °C and annealed there for a long time. However, the POM picture did not change any more (Fig. 8(e)), indicating that PCL blocks crystallized

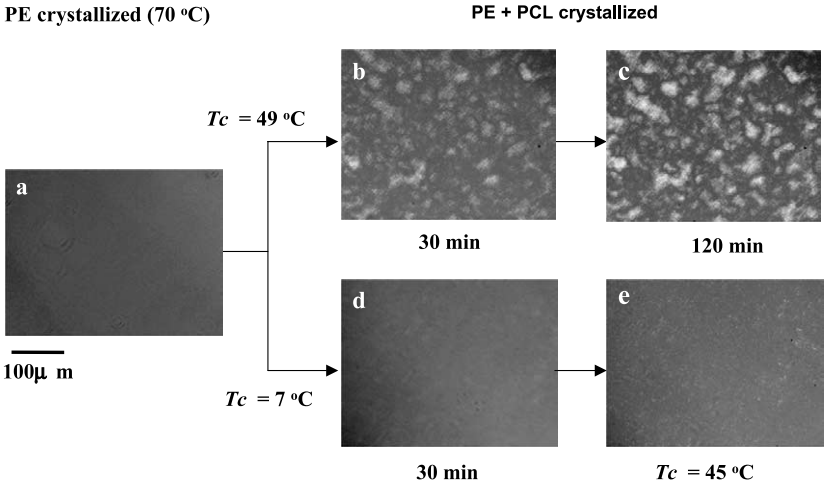

Fig. 8. POM pictures during the crystallization of PCL blocks for A3 at 49 °C (panels b and c) and 7 °C (panel d). Panel e shows the POM picture after A3, crystallized at 7 °C for 30 min, has been brought into 45 °C. The direction of polarizer is horizontal for each picture.

completely at 7 °C and no further crystallization occurred at 45 °C. This fact justifies the DSC results; the morphological transition does not take place during heating process from low T_c, and, therefore, the additional increase in χ_{PCL} will be small even if it exists. Fig. 8 also shows that it would be possible to control the final morphology by changing the thermal history applied to A3; if A3 is directly quenched from the melt into 49 °C we have a morphology mainly driven by the crystallization of PCL blocks, while A3 is first crystallized at 7 °C and then brought into 45 °C, we have a different morphology in which the PE lamellar morphology prevails in the system.

3.5. Factors controlling crystallization behavior

We consider here the difference in factors controlling crystallization behavior between crystalline–amorphous and crystalline–crystalline diblock copolymers. Recently, a change in crystallization mechanism against T_c has been reported for some crystalline–amorphous diblocks, where it is pointed out that the type and the stability of pre-existing microdomains are important factors [25,26]. The stability of microdomains against crystallization is controlled by the total molecular weight of crystalline–amorphous diblocks, where a strongly segregated spherical microdomain, for example, confines the crystallization most effectively.

In crystalline–crystalline diblocks, a solid lamellar morphology certainly exists prior to the second crystallization. The stability of this lamellar morphology solely drives the subsequent crystallization mechanism and resulting morphology, where the stability can be changed by the volume fraction of crystals as well as the total molecular weight. This point is substantially different from the crystallization starting from a rubbery microdomain, where the type of microdomains and total molecular weight (stability of microdomain) affect the subsequent crystallization. Therefore, the solid lamellar morphology formed by the crystallization of high T_m blocks will be a new class of confinement against the subsequent crystallization of low T_m blocks in crystalline–crystalline block copolymers. We are now going to change the volume fraction of PE crystals by synthesizing other PCL-*b*-PE copolymers with different compositions or mixing low-molecular weight PE homopolymers in order to clarify the χ_{PE} dependence of this confinement against PCL crystallization. The result will soon appear.

4. Conclusions

We have investigated the crystallization behavior of PCL blocks in low-molecular-weight PCL-*b*-PE diblocks by DSC, SR-SAXS, and POM, where PCL blocks started to crystallize from a solid lamellar morphology formed in advance by the crystallization of PE blocks. The crystallization behavior was compared with that in PCL-*b*-PB, where the crystallization of PCL blocks started from a rubbery lamellar microdomain to yield a morphological transition into a lamellar morphology at all T_c. Following conclusions were obtained, which are entirely consistent with those previously obtained from static measurements for the final morphology formed at various T_c.

(1) At high T_c, the crystallization of PCL blocks destroyed the PE lamellar morphology, and the crystallization rate was equivalent to that in PCL-*b*-PB. The Avrami exponent was ca. 3 and we could observe a distinct change in POM pictures during the crystallization of PCL blocks. All these results show that PCL blocks crystallize as PCL homopolymers crystallize from the amorphous melt. That is, the crystallization of PCL blocks is not disturbed by the solid pre-existing PE lamellar morphology.
(2) At low T_c, the crystallization rate of PCL blocks in

PCL-*b*-PE was extremely large compared with that in PCL-*b*-PB. The Avrami exponent was significantly smaller, and POM observations showed no macroscopic change in morphology during the crystallization of PCL blocks. This crystallization behavior is consistent with the fact that PCL blocks crystallize within the existing PE lamellar morphology without any morphological transition.

It would be possible to change the crystallization behavior and eventually resulting morphology by changing the stability of the solid PE lamellar morphology, that is, the volume fraction of PE crystals existing in the system.

Acknowledgements

This study was partially supported by NEDO (New Energy and Industrial Technology Development Organization) launched in 2001, and also by Grant-in-Aid for Scientific Research on Priority Area, 'Dynamic Control of Strongly Correlated Soft Materials' (No. 14045225). The SR-SAXS measurement has been performed under the approval of the Photon Factory Program Advisory Committee (Nos. 2002G095 and 2004G093).

References

[1] Nojima S, Kato K, Yamamoto S, Ashida T. Macromolecules 1992;25:2237–42.
[2] Nojima S, Nakano H, Takahashi Y, Ashida T. Polymer 1994;35:3479–86.
[3] Sakurai K, Macknight WJ, Lohse DJ, Schulz DN, Sissano JA. Macromolecules 1994;27:4941–51.
[4] Ryan AJ, Hamley IW, Bras W, Bates FS. Macromolecules 1995;28:3860–8.
[5] Rangarajan P, Register RA, Adamson DH, Fetters LJ, Bras W, Naylor S, et al. Macromolecules 1995;28:1422–8.
[6] Quiram DJ, Register RA, Marchand GR, Ryan AJ. Macromolecules 1997;30:8338–43.
[7] Zhu L, Mimnaugh BR, Ge Q, Quirk RP, Cheng SZD, Thomas EL, et al. Polymer 2001;42:9121–31.
[8] Nojima S, Ono M, Ashida T. Polym J 1992;24:1271–80.
[9] Gan Z, Jiang B, Zhang J. J Appl Polym Sci 1996;59:961–7.
[10] Floudas G, Reiter G, Lambert O, Duinas P. Macromolecules 1998;31:7279–90.
[11] Balsamo V, Muller AJ, Stadler R. Macromolecules 1998;31:7756–63.
[12] Bogdanov B, Vidts A, Schacht E, Berghmans H. Macromolecules 1999;32:726–31.
[13] Shiomi T, Imai K, Takenaka K, Takeshita H, Hayashi H, Tezuka Y. Polymer 2001;42:3233–9.
[14] Balsamo V, Muller AJ, Gyldenfeldt F, Stadler R. Macromol Chem Phys 1998;199:1063–70.
[15] Kim KS, Chung S, Chin IJ, Kim MN, Yoon JS. J Appl Polym Sci 1999;72:341–8.
[16] Kim JK, Park DJ, Lee MS, Ihn KJ. Polymer 2001;42:7429–41.
[17] Albuerne J, Marquez L, Muller AJ, Raquez JM, Degee Ph, Dubois Ph, et al. Macromolecules 2003;36:1633–44.
[18] Bhattarai N, Kim HY, Cha DI, Lee DR, Yoo DI. Eur Polym J 2003;39:1365–75.
[19] Sun J, Hong Z, Yang L, Tang Z, Chen X, Jing X. Polymer 2004;45:5969–77.
[20] Nojima S, Akutsu Y, Washino A, Tanimoto S. Polymer 2004;45:7317–24.
[21] Rohadi A, Endo R, Tanimoto S, Sasaki S, Nojima S. Polym J 2000;32:602–9.
[22] Crescenzi V, Manzini G, Calzolari G, Borri C. Eur Polym J 1972;8:449–63.
[23] Nojima S, Kato K, Ono M, Ashida T. Macromolecules 1992;25:1922–8.
[24] Nojima S, Kikuchi N, Rohadi A, Tanimoto S, Sasaki S. Macromolecules 1999;32:3727–34.
[25] Shiomi T, Takeshita H, Kawaguchi H, Nagai M, Takenaka K, Miya M. Macromolecules 2002;35:8056–63.
[26] Ueda M, Sakurai K, Okamoto S, Lohse DJ, Macknight WJ, Shinkai S, et al. Polymer 2003;44:6995–7005.
[27] Will G, Bellotto M, Parrish W, Hart M. J Appl Crystallogr 1988;21:182–91.
[28] Nojima S, Tsutsumi H, Urushihara M, Kosaka W, Kato N, Ashida T. Polym J 1986;18:451–61.
[29] Wang J, Alvarez M, Zhang W, Wu Z, Li Y, Chu B. Macromolecules 1992;25:6943–51.
[30] Avrami M. J Chem Phys 1939;7:1103–12.
[31] Loo YL, Register RA, Ryan AJ, Dee GT. Macromolecules 2001;34:8968–77.
[32] Zhu L, Cheng SZD, Calhoun BH, Ge Q, Quirk RP, Thomas EL, et al. Polymer 2001;42:5829–39.
[33] Nojima S, Wang D, Ashida T. Polym J 1991;23:1473–82.